Journal of Pharmaceutical Sciences 111 (2022) 69–81

Contents lists available at ScienceDirect

Journal of Pharmaceutical Sciences

journal homepage: www.jpharmsci.org

Pharmaceutics, Drug Delivery and Pharmaceutical Technology

Real-Time Monitoring of Powder Mass Flowrates for Plant-Wide Control of a Continuous Direct Compaction Tablet Manufacturing Process

Yan-Shu Huang[a,*], Sergio Medina-González[a], Benjamin Straiton[b], Joshua Keller[b], Qussai Marashdeh[b], Marcial Gonzalez[c], Zoltan Nagy[a], Gintaras V. Reklaitis[a]

[a] Davidson School of Chemical Engineering, Purdue University, West Lafayette, IN 47907, United States
[b] Tech4Imaging LLC, Columbus, OH 43235, United States
[c] School of Mechanical Engineering, Purdue University, West Lafayette, IN 47907, United States

ARTICLE INFO

Article history:
Received 2 March 2021
Revised 2 June 2021
Accepted 2 June 2021
Available online 12 June 2021

Keywords:
Continuous processing
Process analytical technology (PAT)
Tableting
Powder technology
Quality by Design (QbD)

ABSTRACT

While measurement and monitoring of powder/particulate mass flow rate are not essential to the execution of traditional batch pharmaceutical tablet manufacturing, in continuous operation, it is an important additional critical process parameter. It has a key role both in establishing that the process is in a state of control, and as a controlled variable in process control system design. In current continuous tableting line operations, the pharmaceutical community relies on loss-in-weight feeders to monitor and understand upstream powder flow dynamics. However, due to the absence of established sensing technologies for measuring particulate flow rates, the downstream flow of the feeders is monitored and controlled using various indirect strategies. For example, the hopper level of the tablet press is maintained as a controlled process output by adjusting the turret speed of the tablet press, which indirectly controlling the flow rate. This gap in monitoring and control of the critical process flow motivates our investigation of a novel PAT tool, a capacitance-based sensor (ECVT), and its effective integration into the plant-wide control of a direct compaction process. First, the results of stand-alone experimental studies are reported, which confirm that the ECVT sensor can provide real-time measurements of mass flow rate with measurement error within -1.8 ~ 3.3% and with RMSE of 0.1 kg/h over the range of flow rates from 2 to 10 kg/h. The key caveat is that the powder flowability has to be good enough to avoid powder fouling on the transfer line walls. Next, simulation case studies are carried out using a dynamic flowsheet model of a continuous direct compression line implemented in Matlab/Simulink to demonstrate the potential structural and performance advantages in plant-wide process control enabled by mass flow sensing. Finally, experimental studies are performed on a direct compaction pilot plant in which the ECVT sensor is located at the exit of the blender, to confirm that the powder flow can be monitored instantaneously and controlled effectively at the specified setpoint within a plant-wide feedback controller system.

Introduction

Virtually almost all tablet manufacturing processes today still rely on the batch mode of operation. In the batch mode, materials collected at the end of each batch unit operation are tested off-line before being transferred to the next unit operation to guarantee that the critical quality attributes (CQA) of the samples meet the quality standards approved by regulatory agencies such as the US Food and Drug Administration (FDA) and European Medicines Agency (EMA). While some process analytical technology (PAT) tools have been developed to enable real-time release (RTR) and process control in modern batch processes,[1] batch operations continue to have challenges such as scale-up, high manufacturing cost, and longer processing time.[2,3] For the sake of utilizing raw materials efficiently and avoiding time-consuming off-line tests, the pharmaceutical community is taking steps to shift from batch to continuous operation,[4,5] which requires further advances in real-time process management (RTPM). The key requirements for effective RTPM are to have reliable real-time measurements of the CQAs and critical process parameters (CPP) of the materials being processed, and to use these measurements to design and implement active control strategies for setpoint tracking and disturbance rejection.

* Corresponding author.
E-mail address: huan1289@purdue.edu (Y.-S. Huang).

https://doi.org/10.1016/j.xphs.2021.06.005
0022-3549/

Realizing that increased testing and tight control of process inputs do not necessarily guarantee desired CQAs of in-process materials and final products, the regulatory agencies and the pharmaceutical community have advanced the concept of Quality-by-Design (QbD), which evolved with the ICH Q8 (R2) (Pharmaceutical Development), ICH Q9 (Quality Risk Management), and ICH Q10 (Pharmaceutical Development) guidances.[6] One key point of QbD is that product and process understanding should result in early identification and mitigation of potential sources of variations via appropriate control strategies controlling process outputs. With the aid of PAT tools and process understanding, the systematic design of operating space can be utilized to integrate each unit operation and to enable continuous manufacturing, to achieve reduced manufacturing costs compared to batch process.[7] More recently, the QbD concept has been extended to a new concept called Quality-by-Control (QbC), aimed at addressing the issues caused by process disturbances and uncertainties as well as at providing more efficiency and robustness than QbD approaches.[8] The advantages of the QbC method are achieved as a result of applying active control strategies. Some examples of implementation of active control strategies in the direct compaction process include API concentration controlled by a hybrid MPC-PID control structure,[9] and variations of tablet weight significantly reduced by a control framework comprised of MPC and data reconciliation.[10]

In continuous operation, the mass flow rate is an important CPP, which is typically not required in batch processing. Mass flow rate not only can serve as a direct indicator of whether the process is in a state of control but also as one of the directly controlled variables in the process control system design. Directly controlled variables are variables that can be controlled based on their real-time measurements. For instance, the API concentration can be directly controlled by adjusting the API flow rate. On the other hand, some important variables need to be controlled indirectly because their real-time measurements are missing or difficult. For example, the dissolution of the tablet is maintained within the target range indirectly by controlling the tablet weight and compression force. Due to the absence of established measurements of intermediate process flows, the most common indirect control strategy is to adjust the turret speed of the tablet press frequently so as to maintain the hopper level of the tablet press as a controlled variable that can be monitored in real time.[11,12] Yet, variations in turret speed are well-known to have the potential to cause undesirable variations in tablet properties. While many PAT tools have been used to measure the composition and selected material properties of particulate process streams, at present, process flows are only obtained from loss-in-weight (LIW) feeders and these only provide process input stream flow rates. LIW feeder flow rates can be compromised when the sudden change of the powder weight (e.g. refilling) and unexpected events (e.g. powder ratholing, bridging, agglomeration) occur. To mitigate process variations and disturbances caused by such risk scenarios, closed-loop feedback control is required. However, powder flow dynamics can not be managed in an active feedback control loop without the real-time measurements of the intermediate powder flow rate. Therefore, the investigation of real-time flow measurements of intermediate particulate streams is relevant and appropriate for RTPM of continuous processes.

To date, relatively few PAT tools have been reported for real-time mass flow monitoring of particulate streams. An X-ray-based sensor has been the first reported PAT tool used for on-line mass flow monitoring in continuous tableting.[13] The report indicated that powder flow could be measured by the X-ray sensor with a measurement error of 5%. However, there may exist potential safety concerns with the use of X-ray in a process environment and the constraints on sensor location caused by the required bulky lead shielding. Another camera image-based measurement system has been reported to be the first PAT tool used to monitor and control ultra-low dose powder feeding.[14] The limitations of the camera image-based sensor are particle image enlargement caused by defocusing as well as underestimated volume fraction due to overlapping particle images. In addition, Terahertz (THz) technology has been reported to measure the powder bulk density and predict the fill weight of capsules,[15] demonstrating the potential to measure real-time mass flow rate in the future. On the other hand, capacitance-based sensors are widely used in systems involving pneumatically conveyed particles,[16–18] but are rarely used in the pharmaceutical industry. Yan reported that the capacitance-based sensor is not influenced by variations in particle size but is sensitive to variations of moisture content.[19] In this study, a novel capacitance-based sensor will be investigated.

Electrical Capacitance Volume Tomography (ECVT) is a process tomography modality that was introduced in 2007 by Warsito, Marashdeh, and Fan.[20] ECVT is a volumetric extension of Electrical Capacitance Tomography (ECT) that uses additional information collected from non-linear three-dimensional plate-pair geometries to reconstruct images of a region of interest. ECVT is quickly becoming of interest to the process industry due to its adaptability, low power consumption, non-invasiveness, safety, and high acquisition speed. ECVT is highly adaptable to industrial processes because it utilizes a passive set of electrodes which are placed around the pipe or other region of interest. These passive electrodes can be used in high temperatures,[21] large scale,[22] and regions of odd geometries.[23,24] The technology was primarily developed for gas-solid flows[25,26] but was later adapted to air-liquid flows[27,28] and even three-phase flows.[29,30] ECVT has been verified against magnetic resonance imaging (MRI),[31,32] optic probes,[33] and CPFD software.[34] In the next section, the ECVT system we used will be described in more detail.

ECVT for Real-Time Mass Flow Monitoring

Sensor Description

The ECVT sensor, offered by Tech4Imaging LLC, (Columbus, OH), is a non-invasive sensing technology with fast data acquisition. The compact size of the ECVT sensor ensures the simple installation of the sensor on the pipe or transfer line. Also, the dimension and structure of the sensor can be designed according to the targeted application. Two kinds of sensor structures are used in this study. As shown in Fig. 1a, one sensor structure has an inner diameter of 1 inch and consists of 4 plates, where plate 1 and plate 2 are viewed as a top parallel-plate capacitor, and plate 3 and plate 4 are considered as a bottom parallel-plate capacitor. The other sensor structure as indicated in Fig. 1b has an inner diameter of 2.75 inch and is composed of 12 small plates, where 4 of those 12 plates are disconnected (small plates #3,6,9,12 as shown in Fig. 1c) and each 2 small plates of the other 8 plates are combined into a large plate (small plates #1,2 form large plate 1, small plates #4,5 form large plate 2, small plates #7,8 form large plate 3, and small plates #10,11 form large plate 4, as shown in Fig. 1c). Similarly, the top 2 plates function as a top parallel-plate capacitor and the bottom 2 plates serve as a bottom parallel-plate capacitor.

Sensor Principle

Due to complex properties of powder flow, it is more difficult to measure the mass flow rate of particulate stream than that of fluid

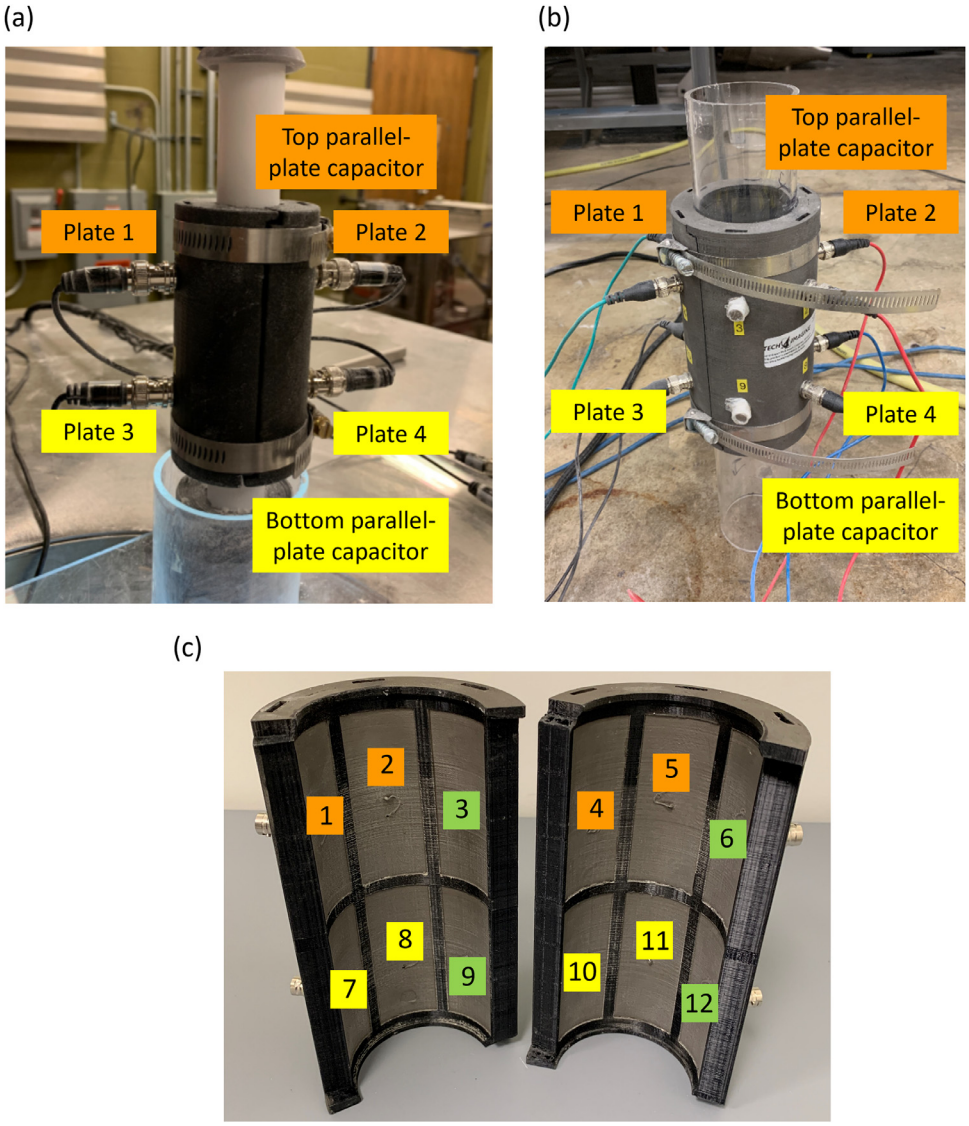

Fig. 1. ECVT sensor with the inner diameter of (a) 1 inch and (b) 2.75 inch and (c) details of the 12 small plates of the 2.75 inch sensor.

stream. Typically, the inferential method[19] including measurement of instantaneous particle velocity and instantaneous volume fraction is used to deduce the mass flow rate of solids as shown in

$$M_s = \rho_{ts} A V_s \beta_s \tag{1}$$

where M_s is the mass flow rate of solids, V_s is the velocity of solids, and β_s is the volume fraction of solids. True density of solids ρ_{ts} can be assumed to be a constant and the cross-sectional area A of the pipe is known.

The ECVT sensor is based on the principle of parallel-plate capacitor as represented by Eq. (2) where the dielectric permittivity of dilute solid-gas mixtures can be defined by Eq. (3).[35]

$$C = \varepsilon \frac{A_p}{d} \tag{2}$$

$$\varepsilon = \beta_s \varepsilon_s + (1 - \beta_s) \varepsilon_{air} \tag{3}$$

where ε, ε_s and ε_{air} are the permittivity of mixture, solids and air respectively. C is capacitance, A_p is the area of the plate, d is the distance between two plates, β_s is the volume fraction of solids, and (1-β_s) is the volume fraction of air. A higher mass flow rate is reflected in higher permittivity and thus capacitance.

Instead of providing actual values of capacitance or permittivity, the ECVT sensor in fact provides the normalized capacitance as shown in Eq. (4).

$$C_n = \frac{I_{measured} - I_{empty}}{I_{full} - I_{empty}} = \frac{1}{k} \frac{C - C_{air}}{C_s - C_{air}} = \frac{1}{k} \beta_s \tag{4}$$

where intensity (I) is an integer value between −65,536 and 65,535 and k is a scaling factor. During the initial calibration procedure of the sensor, the normalized capacitance of the empty pipe is 0 and that of the pipe full of solid powders is 1. The measurement of the powder velocity is based on the cross-correlation velocimetry as represented by Eq. (5) where L is the axial distance between the top parallel-plate capacitor and the bottom parallel-plate capacitor. The value τ is the time delay between signals from the top capacitor and the bottom capacitor. If considering the known sensor length and expected velocity of the powders, the

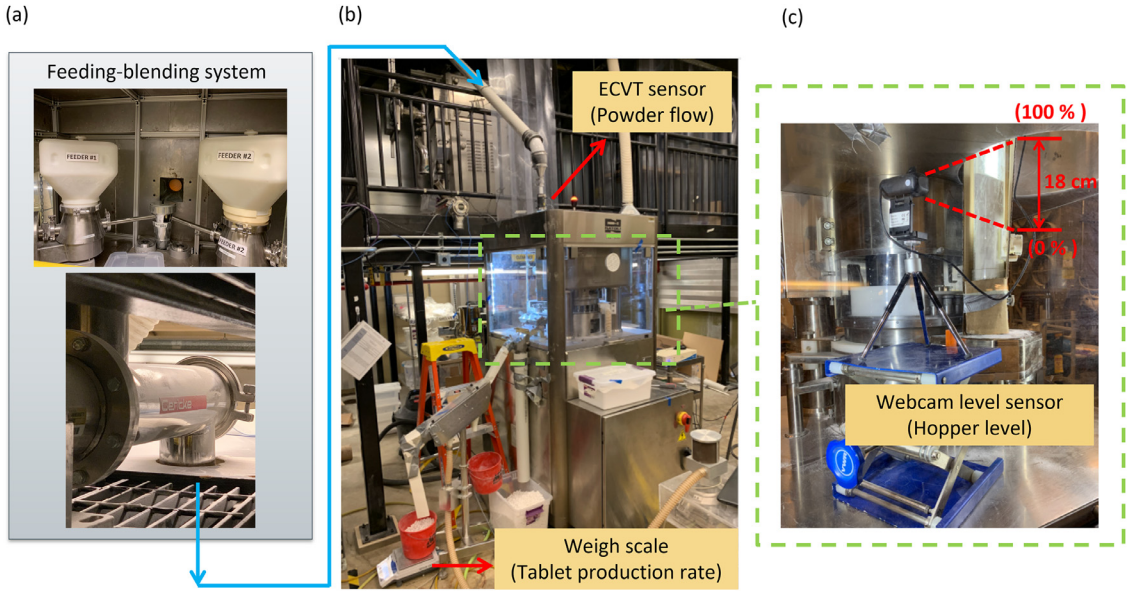

Fig. 2. Unit operations in the direct compaction line including (a) loss-in-weight feeders and the continuous blender, (b) the tablet press with the ECVT powder mass flow measurement at the inlet and weigh scale-based tablet production rate measurement at the outlet, and (c) the hopper associated with the tablet press with a camera and image analysis-based level measurement system.

time window size T is set to be around 5 times the expected time delay.

$$V_s = \frac{L}{\tau} = \frac{L}{\arg\max_\tau \int_{t_0}^{t_0+T} C_{n,top}(t) C_{n,bottom}(t-\tau) dt} \quad (5)$$

Signal Processing

There are various forms of electrical capacitance sensing including charge-discharge and alternating current (AC). In both cases, the standing capacitance of a sensor can be quite large compared to the low changes in capacitance which are tied to the flow behavior in the region of interest. Because of this, complex circuitry can be employed to cancel out or balance the signal using direct current (DC) offset or AC feedback. Additionally, stability of the analog circuits can pose a large problem for repeatable resolution. Small changes in the thermal dissipation of the circuits for the Data Acquisition System (DAS) can cause large changes in measured capacitance. Two solutions are employed to mitigate these thermal effects, good circuit design to minimize the effect of thermal dissipation induced drift and temperature correction which utilizes on board temperature sensors and reliable system testing to correct any residual thermal effects. This is critical in the present application because the detected change in capacitance is so low that any small thermal drift could produce large relative errors in measurement. The AC-based DAS used in this paper was tested extensively to generate temperature correction curves to eliminate drift to a satisfactory level. The detailed experimental results are described in Supplementary Information S1.

Implementation Components

Materials

Acetaminophen Grade 0048 (APAP) was purchased from Mallinckrodt (Raleigh, NC, USA). Avicel microcrystalline cellulose Grade PH-102 (MCC-102) and Grade PH-200 (MCC-200) were purchased from FMC BioPolymer (Philadelphia, PA, USA). Lactose monohydrate Grade 310 was purchased from Kerry Inc. (Jackson, WI, USA). Magnesium stearate (MgSt) was used as lubricant. Cab-O-Sil M5P nano-sized silica (nominal size 20 nm) was purchased from Cabot (Tuscola, IL, USA). All 3 kg powder blends were prepared by using a 5 L Tote blender for 30 min.

Stand-Alone Configuration for Sensor Investigation

A stand-alone configuration consisting of a K-Tron KT20 loss-in-weight (LIW) feeder, the ECVT sensor, and an independent Mettler-Toledo ME 4001E weighing scale for gravimetric measurement. The goal of this setup is to investigate the sensor more efficiently using a minimum amount of powder blend before the integration of the sensor into the DC line. At each measurement, one minute of no flowing material at the beginning and in the end are used to detect the extent of measurement drift and fouling.

Integration of PAT Tools in the DC Line

To verify the control performance with the aid of mass flow sensing, the control structure and the ECVT sensor are implemented in the continuous direct compaction line at Purdue University's pilot plant. The feeding-blending system (Fig. 2a) consists of two Schenck AccuRate PureFeed® AP-300 loss-in-weight (LIW) feeders that dispense the API and the excipient respectively into the Gericke GCM-250 continuous blender. The commercial-scale tablet press Natoli NP-400 has 22 stations with concave-head punches (Fig. 2b). The blender and the tablet press are connected by the following order: the pipe with inner diameter of 3 inch at 45° angle, a pipe elbow, a concentric reducer, and the 1 inch PTFE pipe, where the ECVT sensor is installed to capture the real-time powder flow. At the exit of the tablet press, the tablets are collected in a bucket on the Mettler-Toledo ME 4001E weighing scale and the real-time tablet production is measured. Inside the chamber of the tablet press, a webcam-based level sensor is located to monitor the powder level in the hopper, which is a 2.5 inch acrylic pipe (Fig. 2c). The range of the hopper level is limited by the camera view and can be defined by users. In the experimental case studies, 0% and 100% correspond to 0 cm and

Table 1
Powder Properties (All Data are Cited from Li, 2019).

	MCC-102	MCC-200	Lactose 310	APAP	MgSt
d_{10} (μm)	37.8	45.3	18.6	9.9	4.5
d(3,2) (μm)	74.6	74.0	34.9	23.5	8.8
d_{50} (μm)	124.7	143.7	82.7	57.4	12.1
d_{90} (μm)	245.3	195.1	176.3	166.0	23.5
Aerated bulk density (g/cm^3)	0.320	0.331	0.685	0.350	0.160
Tapped density (g/cm^3)	0.440	0.417	0.885	0.580	0.230
Hausner Ratio	1.38	1.26	1.29	1.67	1.44
Cohesion (kPa)	0.163	0.077	0.220	0.670	0.363
Flow function coefficient	10.28	26.27	6.60	2.59	4.43
Jenike flow function	7.79	18.23	4.98	2.16	3.19

18 cm respectively. It must be noted that 0% means the lowest part of the hopper that the camera can image rather than indicating that the hopper is empty and out of materials.

To transmit the real-time PAT measurements to the distributed control system (DCS) DeltaV, OPC communication protocols are established between PAT laptops and the DCS. All the process variables have the sampling time of 1 second in the DeltaV continuous data historian. For the API and excipient flowrates, a moving average window of 7 s is used for the raw measurements, while the total blend flow has a 5 second average window and the tablet production rate has a 10 second average window.

Results and Discussion

ECVT Sensor Calibration and Stand-Alone Performance

To calibrate the sensor and understand the sensor performance in real-time mass flow monitoring, a stand-alone system was used. The powder properties for the materials processed are provided in Table 1, all cited from Li's work.[36] The MCC-200 data does indicate that it has the best flowability, supported by the smallest Hausner Ratio, the largest flow function, and the largest coefficient, and Jenike flow function. To further improve powder flowability and thus reduce the negative influence of powder fouling on flow measurement, glidant (silica) and lubricant (MgSt) have been added.

When one model material (MCC-200 with 0.2% Silica and 0.5% MgSt) was delivered through a 1 inch PTFE pipe, the resulting real-time normalized capacitance was shown in Fig. 3a. The reason for adding glidant and lubricant to MCC-200 was to guarantee that a perfect flowing material is used during the stand-alone sensor investigation. If the sensor measurement was still not satisfactory, it might mean that further improvements in the sensor technology may be required. Given that the powders were falling freely by gravity, the terminal velocity was independent of the mass flow rate and assumed to be a constant. To calibrate the ECVT sensor, the average capacitance over a minute and the corresponding average flow rates from the weighing scale were used to perform linear regression as represented by Fig. 3b. The reason for utilizing average data was that the buoyancy and the drag force caused by the upward air flow made it challenging to know the actual point-by-point flow rate of the powder in the pipe. With the linear regression model whose R^2 is 0.9863, the real-time mass flow rate can be predicted from the real-time capacitance as shown in Fig. 3c.

Powder bulk density, particle size, and API concentration are all common sources of process variability. To investigate the effects of these three powder properties, tests were conducted with the five types of powders including (1) Lactose, (2) MCC-102, (3) MCC-200, (4) 90% MCC-200 + 10% APAP MCC-200, and (5) 80% MCC-200 + 20% APAP. The capacitance, velocity, and the predicted mass flow rate are shown in Fig. 4 and the measurement performances are summarized in Table 2. First, the effects of bulk density were observed from the results of MCC-102 (0.320 g/cm^3) and those of lactose (0.685 g/cm^3). At the same screw speed, lactose was dispensed at a higher mass flow rate and higher velocity than MCC-102. The highest velocity of lactose among all materials resulted in the lowest capacitance. The errors of mass flow rate were similar in both materials, indicating that the accuracy of mass flow rate should not have a strong

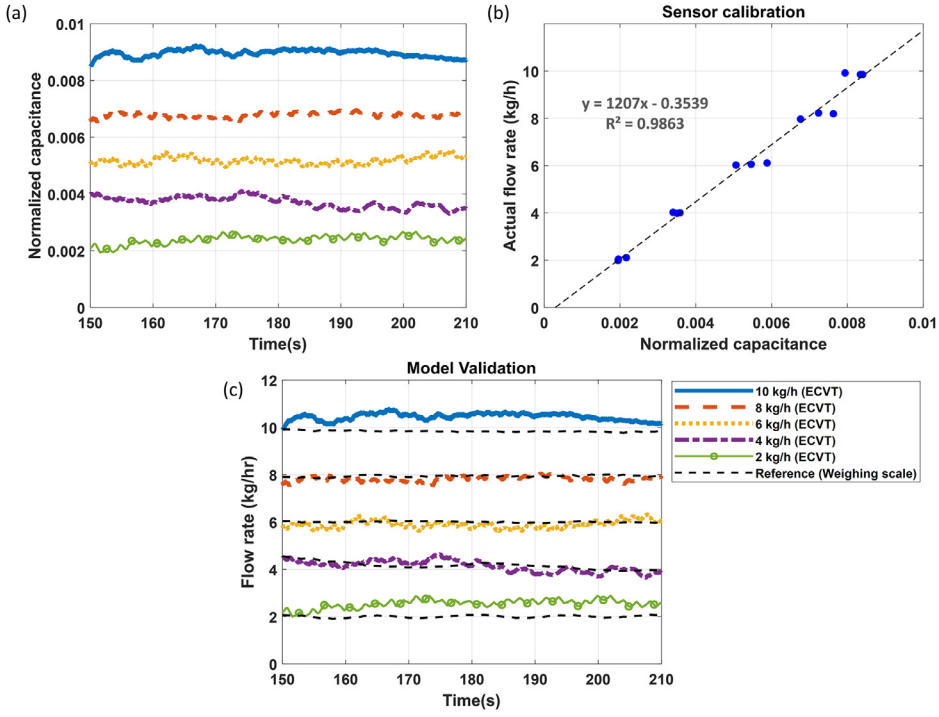

Fig. 3. Sensor calibration including (a) time-series capacitance, (b) average capacitance used for calibration, and (c) time-series predicted mass flow rate.

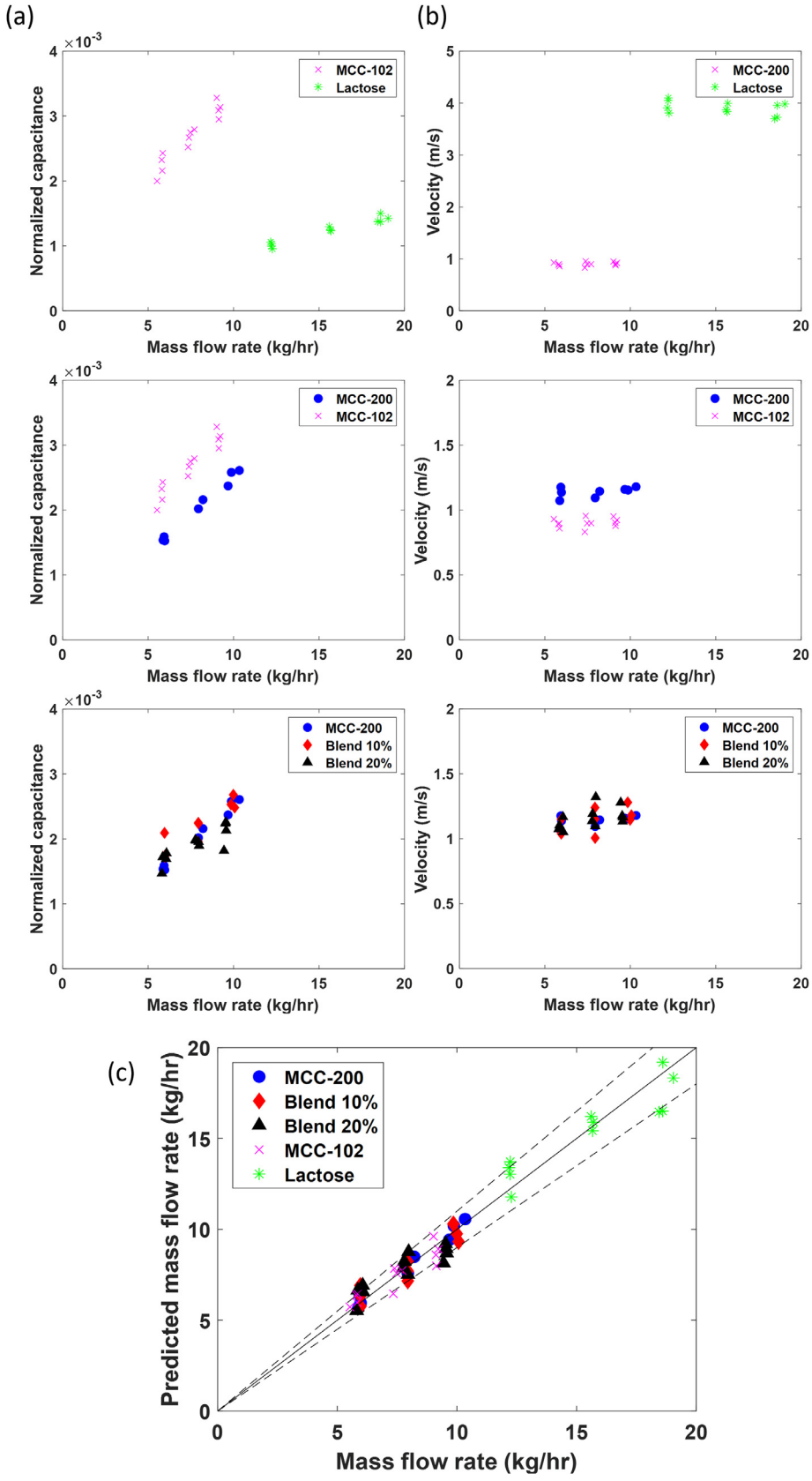

Fig. 4. Effects of powder properties including bulk density, particle size and concentration of API on (a) normalized capacitance, (b) velocity and (c) predicted mass flow rates.

Table 2
Average Errors of the Predicted Mass Flow Rates from the ECVT Sensor.

Pipe	Powder Material	Flow Range (kg/h)	Average Error (%)	RMSE (kg/h)
2.5″ Acrylic	MCC-200	6 ~ 10	−4.5 ~ 7.7	0.29
	Blend 10%	6 ~ 10	−7.4 ~ 15.9	0.54
	Blend 20%	6 ~ 10	−13.8 ~ 14.1	0.68
	MCC-102	6 ~ 10	−12.6 ~ 10.0	0.56
	Lactose	12 ~ 20	−11.2 ~ 12.2	1.14
1″ Polycarbonate	MCC200 + 0.2% silica	2 ~ 10	−10.0 ~ 3.9	0.41
1″ PVC	MCC200 + 0.2% silica	2 ~ 10	−8.5 ~ 5.6	0.32
1″ PTFE	MCC200 + 0.2% silica	2 ~ 10	−1.8 ~ 3.3	0.10
	MCC200 + 0.2% silica +0.5% MgSt	2 ~ 10	−7.8 ~ 10.4	0.35

dependence on bulk density. Secondly, effects of particle size were noticed from the results with MCC-200 (median size ~ 143.7 μm) and those of MCC-102 (median size ~ 124.7 μm). At the same mass flow rates, the velocity of MCC-102 (0.9 m/s) was slightly smaller than that of MCC-200 (1.1 m/s) due to size effects.[37] The volume fraction was inversely proportional to the velocity, which was verified by the fact that the capacitance of MCC-102 was larger than that of MCC-200. The higher RMSE (0.56 kg/h) of mass flow rate of MCC-102 than of MCC-200 (0.29 kg/h) may be attributed to fouling caused by poor flowability of the material with smaller particle size. Thirdly, effects of the API concentration were observed from the results of MCC-200, Blend 10% (10% APAP + 90% MCC-200) and Blend 20% (20% APAP + 80% MCC-200). The velocity of these three materials was similar at the same mass flow rates. However, the error in the capacitance and mass flow rates of Blend 10% and Blend 20% were higher than those of MCC-200, which may be attributed to content uniformity of APAP in blends and different permittivity of MCC-200 and APAP. Although all the results shown in Fig. 4 are collected using powders without glidant or lubricant, these constituents can be added to further improve the flowability of MCC-102, lactose, APAP, or the blend with APAP. Assuring that every powder has good flowability is beyond the scope of this study.

Fouling was a key factor in deteriorating the sensor accuracy, and it is known that adhesivity and electrostatic chargeability of the powders are two main reasons for fouling.[38] Accordingly, the effects of pipe materials were investigated including PTFE (friction coefficient: 0.04, work function: 5.75 eV), PVC (friction coefficient: 0.20, work function: 5.13 eV), and polycarbonate (friction coefficient: 0.31, work function: 4.68 eV). Providing that pipes with lower friction coefficient can reduce the amount of powder that adheres to the pipe wall, PTFE was the best candidate. In addition, given that larger difference in work function between two materials will result in more accumulated static charges and that the work function of MCC is 5.11 eV, PVC was the best candidate. When MCC-200 with 0.2% silica was delivered through these three pipes, PTFE demonstrated the lowest RMSE as shown in Table 2. These results indicate that fouling of MCC-200 is more subject to the friction coefficient than to the work function. Therefore, the PTFE pipe should be used if MCC-200 accounts for a large percentage.

These stand-alone studies indicated that the ECVT could provide mass flow measurements with suitable accuracy and precision. In this work, the frequency of raw flow measurement was 10 points per second, and measurement noise was reduced using the moving average filter with 5 seconds window, which did not compromise on capturing the fast dynamics of tablet manufacturing process. Hence, the real-time flow measurements are proper for process control and plant-wide control design will be discussed in the next section.

Plant-Wide Control Design

Process control systems are designed to serve as an automated means of mitigating a wide range of common cause variations in material and process parameters. According to the ISA-95 Enterprise-Control-System Integration Standard,[39,40] the hierarchical three-level control structure is employed in modern control system implementation with the levels classified according to their control objectives.[8] More detailed descriptions of ISA standards for control design in pharmaceutical continuous manufacturing are reported in our previous work.[41] The level 0 control involves equipment-based control, in which programmable logic control (PLC) panel in the equipment is used to manipulate CPPs directly to control basic equipment operating variables such as rpm or pressure. The level 1 control is PAT-based property feedback control. For instance, the cascaded Single-Input Single-Output (SISO) loops with PID controllers can be used to control CQAs based on measurements from PAT tools. The level 2 control is often implemented using optimization-based model predictive control of the entire integrated production line. The control system designs considered in this study are limited to the level 0 and level 1 control functions. It should be noted that the aforementioned three-level control structure used in this study is different from the three-level control strategy for quality control defined by the FDA,[5] in which level 3 is traditional control, level 2 is pharmaceutical control and level 1 is engineering control.

The weight measurement is crucial for the level 0 PLC of LIW feeders to maintain the desired mass flow. The refilling process and unexpected events such as powder ratholing can cause variations in the mass flow rate. Moreover, the vibration in the feeder caused by the screw rotation can disturb the load cell measurement frequently and result in the calibration error of the LIW feeder itself. To investigate the ability to handle risk scenarios caused by LIW feeders, three control structures are considered as shown in Fig. 5:(a) process with only level 0 (open-loop) control, (b) process with level 1 PID closed-loop control using only the API composition measurement at the exit of the blender, which is the most common feedback control structure reported in the literature,[11,42,43] and (c) level 1 PID closed-loop control using the measurements of both the API concentration and the powder flowrate at the exit of the blender, which is the case study to show the benefits of mass flow sensing. The only distinction between the second and the third cases is the existence of the blend flow control loop. The tablet press is controlled by the same level 1 PID controllers in both cases. The detailed control pairings of six inputs and six outputs for level 1 supervisory control are listed in Table 3, in which the controlled variable y_i is maintained by adjusting the manipulated valuable u_i.

Dynamic flowsheet models can serve as digital surrogates for a real manufacturing process, so that evaluation of control strategies and the risk analysis can be done before the actual implementation of the physical process. The process model equations, described in Supplementary Information S2, are written in Matlab S-function files and thus can be executed in the Simulink environment. In addition to using the process model to study control configurations and system response to a variety of disturbances, the process model can also be used to study the interaction among the set of system input and output variables so as to extract insights into input-output variable

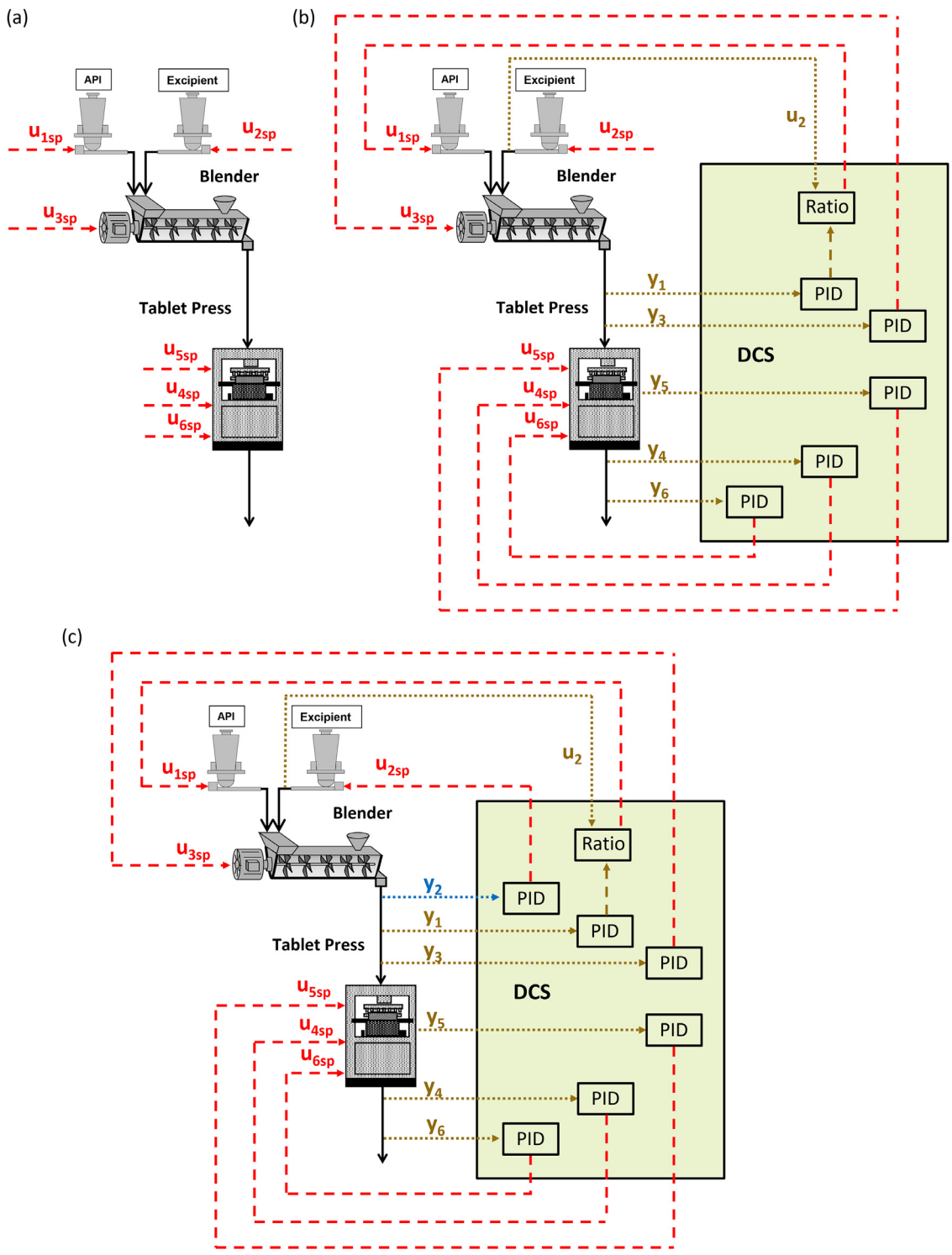

Fig. 5. Three control structures including (a) level 0 open-loop, (b) level 1 closed-loop without total flow control, and (c) level 1 closed-loop with total flow control. (subscript sp means the setpoint).

pairings and inherent control system stability. For example, providing both excipient flow rate and API flow rate can affect the intermediate process flow and the API concentration, the input-output variable pairings need to be determined in control design. In this study, the interactions and relative stability of Multi-Input Multi-Output (MIMO) system configurations are carried out using the well-established relative gain array (RGA) analysis, a well-established approach to interactions analysis. RGA is defined as the ratio of an open loop gain to the same closed-loop gain when the other loops are under perfect control. The elements in the array indicate the process interaction, including (a) the range 0 to 1 means moderate interaction, (b) the value greater than 5 means severe interaction, and (c) negative values means unstable system.[44] Also, the relative gain closest to 1 implies the paired single-input single-output (SISO) control loop is almost unaffected by closing the other control loops. The RGA is computed using the equations below.

Table 3
Process Variables and Supervisory Control Schemes.

Critical Process points	Model Output (y) Controlled Variables	Model Input (u) Manipulated Variables	Supervisory Scheme
Blender	API Composition (y_1)	API flow rate (u_1)	PID + ratio
	Powder flow (y_2)	Excipient flow (u_2)	PID
	API RSD (y_3)	Blender rotation speed (u_3)	PID
Tablet press	Tablet weight (y_4)	Dosing position (u_4)	PID
	Main compression force (y_5)	Main thickness (u_5)	PID
	Production rate (y_6)	Turret speed (u_6)	PID

$$G(s) = C(sI - A)^{-1}B + D \tag{6}$$

$$\Lambda = G(s=0) \odot \left(G^{-1}(s=0)\right)^{T} \tag{7}$$

where G(s) is the system transfer function matrix. *A, B, C*, and *D* are the matrices in the state-space model, which can be easily computed using the Matlab Control System Toolbox (right clicking the interested system in the Simulink, then choosing "Linear Analysis → Linearize Block"). The *I* is the identity matrix, Λ is the RGA matrix and G(s = 0) is the steady-state gain matrix. $\odot$ is the operator for Hadamard product, also known as element-wise product. When the RGA element (i,j) in the *i*th row and the jth column is close to 1, this indicates that the *i*th output and the *j*th input is the preferred control-loop pairing.

Simulation-Based Assessment of Control Performance Under Risk Scenarios

Without loss of generality, a calibration error of −20% is introduced in the process simulation in the excipient LIW feeder at t = 300 s to represent the risk scenario as shown in Fig. 6. In addition to typical integral of time absolute error (ITAE), some additional metrics are used to quantify the control performance, including out-of-specification (OOS) time, duration-to-reject (D2R), and magnitude-to-product (M2P).[45] Specifically, OOS time means the period during which the CQA is outside of the tolerance limits. D2R is the duration of time that the process requires to smooth out the process disturbance or to reach a new set point for the CQA. M2P describes the maximum deviation in the CQAs from the target setpoint, which takes place. The lowest values of the above indicators are preferred. The evaluations of control performance in terms of these metrics and based on the API composition and the tablet weight are summarized in Table 4.

Under the risk scenario of a calibration error in the feeder, the level 0 open-loop control fails to maintain the API concentration, the powder flow rate, and the tablet weight at the target values. In addition, the tablet press hopper level drops significantly from 50% to 23.2%, which may cause the potential risk of a shortage of powders. By contrast, both level 1 closed control loops can correct the API concentration back to the ± 5% tolerance limit and maintain the tablet weight within 0.11% error. Moreover, the closed loop with both API

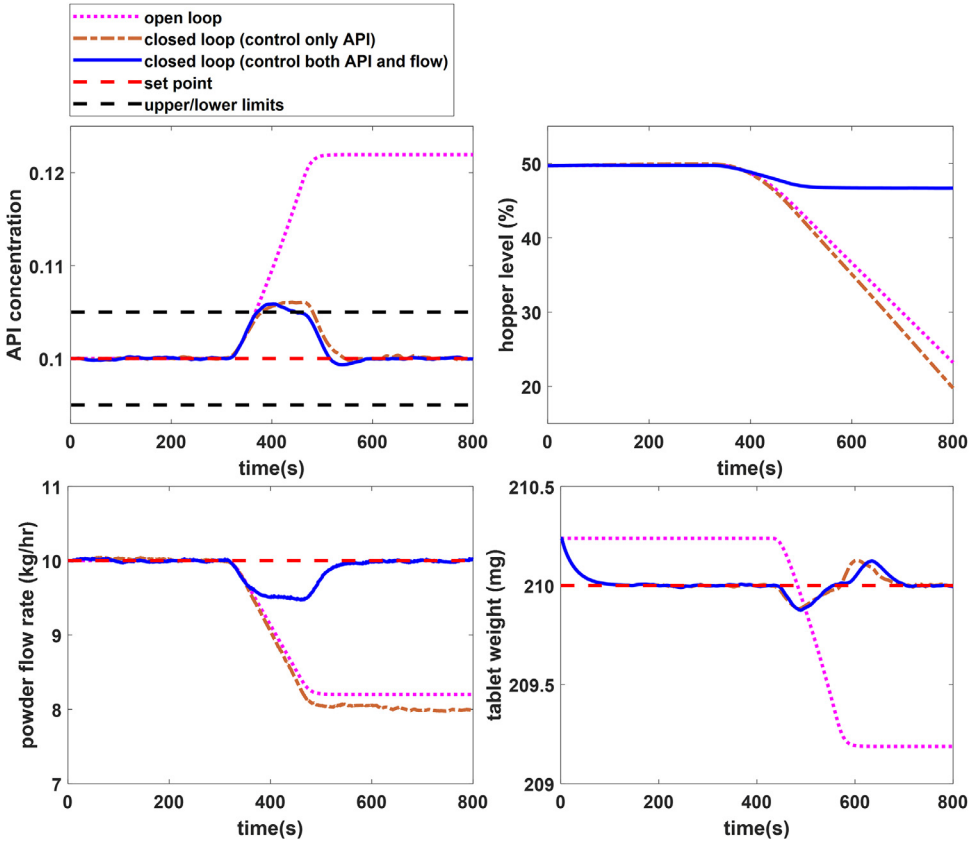

Fig. 6. Control performance when the calibration error occurs to the LIW feeders.

Table 4
Performance Evaluation Based on API Composition and Tablet Weight.

CQA	Performance Indicators	L0 Open Loop	L1 Closed Loop Without Flow Sensing	L1 Closed Loop With Flow Sensing
API concentration	OOS time(s)	Fail	102	72
	D2R (s)	Fail	245	211
	M2P (%)	22	6.1	5.9
Tablet weight	D2R (s)	Fail	270	270
	M2P(%)	0.24	0.11	0.11
	ITAE (s)	809.3	46.4	44.2

concentration and flow control exhibits better control performance than the closed-loop with only API concentration control, given smaller M2P, D2R, and ITAE value. When the API composition is beyond 5% control limits, the OOS materials/products must be diverted. In other words, PID with mass flow control will require rejection of approximately 950 tablets over the OOS time of 72 s (from t = 373 s to 445 s), saving more materials compared to PID without mass flow control which requires rejection of 1350 tablets in the OOS time of 102 s (from t = 380 s to t = 482 s). From the viewpoint of hopper level, PID with both API concentration and flow control keeps the hopper level within 3.3%, which is obviously better than PID with only API concentration control. Therefore, the additional PAT tool for mass flow sensing can make the control strategy more robust under these risk scenarios.

Relative gain array analysis

The interaction analysis for the multi-input multi-output (MIMO) system is carried out using the relative gain array (RGA) analysis. Given 6 inputs and 6 outputs in the system as previously shown in Table 3, the RGA results of 6 × 6 dimension for the direct compaction process with different target API concentrations are shown in Fig. 7. When the target API concentration is 10% or 30%, the RGA indicates that the diagonal pairing should be used because these six diagonal values are close to 1, suggesting that this MIMO system can be decoupled into multiple SISO loops. However, when the target API concentration is 50%, the value 0.5 is the worst case of moderate interaction (range 0 to 1).[44] The case of 70% API concentration has the opposite control parings for feeders compared to the case of 30% API concentration. Overall, the larger concentration difference between the API and the excipient makes it easier to decouple the MIMO system into several SISO loops. In this study, the 10% API concentration is the target value and that experimental implementation will be demonstrated in the next section.

Experimental case study 1: only the excipient was delivered

Fig. 8a provides the reading of the excipient feeder and Fig. 8b presents the ECVT measurement of the total flow exiting the blender. The excipient (MCC-200 pre-blended with 0.5 wt% MgSt and 0.2 wt% silica) was dispensed at 7 kg/h during the level 0 open-loop operation. When the level 1 control was applied at time = 300 s, the deviation in the powder flow from the setpoint was mitigated, as indicated by a decrease in the average absolute error from 0.41 kg/h (time = 100 ~ 200 s) to 0.26 kg/h (time = 350 ~ 450 s). In addition, a step change from 7 kg/h to 9 kg/h at time = 500 s was well performed with a single loop level 1 PID controller.

The hopper level (as shown in Fig. 9d) was almost fixed as the total powder flow (as shown in Fig. 9c) was equal to the tablet production rate. While the production rate was intentionally increased to be larger than the powder flow rate (time = 400 ~ 550 s), the hopper level was decreased accordingly. It is interesting to note that during one of the runs an internal alarm stopped the tablet press and thus the production rate dropped to 0 kg/h at time = 580 s. Taking advantage of the real-time monitoring of both the powder flow and the hopper level, the remaining process equipment did not have to be shut down to prevent excessive powder accumulation before the tablet press was restarted again. Besides, the hopper level can be

10% API

	u1	u2	u3	u4	u5	u6
y1	**0.90**	0.10	0.00	0.00	0.00	0.00
y2	0.10	**0.90**	0.00	0.00	0.00	0.00
y3	0.00	0.00	**1.00**	0.00	0.00	0.00
y4	0.00	0.00	0.00	**0.98**	0.00	0.02
y5	0.00	0.00	0.00	0.00	**1.00**	0.00
y6	0.00	0.00	0.00	0.02	0.00	**0.98**

30% API

	u1	u2	u3	u4	u5	u6
y1	**0.70**	0.30	0.00	0.00	0.00	0.00
y2	0.30	**0.70**	0.00	0.00	0.00	0.00
y3	0.00	0.00	**1.00**	0.00	0.00	0.00
y4	0.00	0.00	0.00	**0.98**	0.00	0.02
y5	0.00	0.00	0.00	0.00	**1.00**	0.00
y6	0.00	0.00	0.00	0.02	0.00	**0.98**

50% API

	u1	u2	u3	u4	u5	u6
y1	**0.50**	**0.50**	0.00	0.00	0.00	0.00
y2	**0.50**	**0.50**	0.00	0.00	0.00	0.00
y3	0.00	0.00	**1.00**	0.00	0.00	0.00
y4	0.00	0.00	0.00	**0.98**	0.00	0.02
y5	0.00	0.00	0.00	0.00	**1.00**	0.00
y6	0.00	0.00	0.00	0.02	0.00	**0.98**

70% API

	u1	u2	u3	u4	u5	u6
y1	0.30	**0.70**	0.00	0.00	0.00	0.00
y2	**0.70**	0.30	0.00	0.00	0.00	0.00
y3	0.00	0.00	**1.00**	0.00	0.00	0.00
y4	0.00	0.00	0.00	**0.98**	0.00	0.02
y5	0.00	0.00	0.00	0.00	**1.00**	0.00
y6	0.00	0.00	0.00	0.02	0.00	**0.98**

Fig. 7. RGA analysis for the direct compaction process with different target API concentrations.

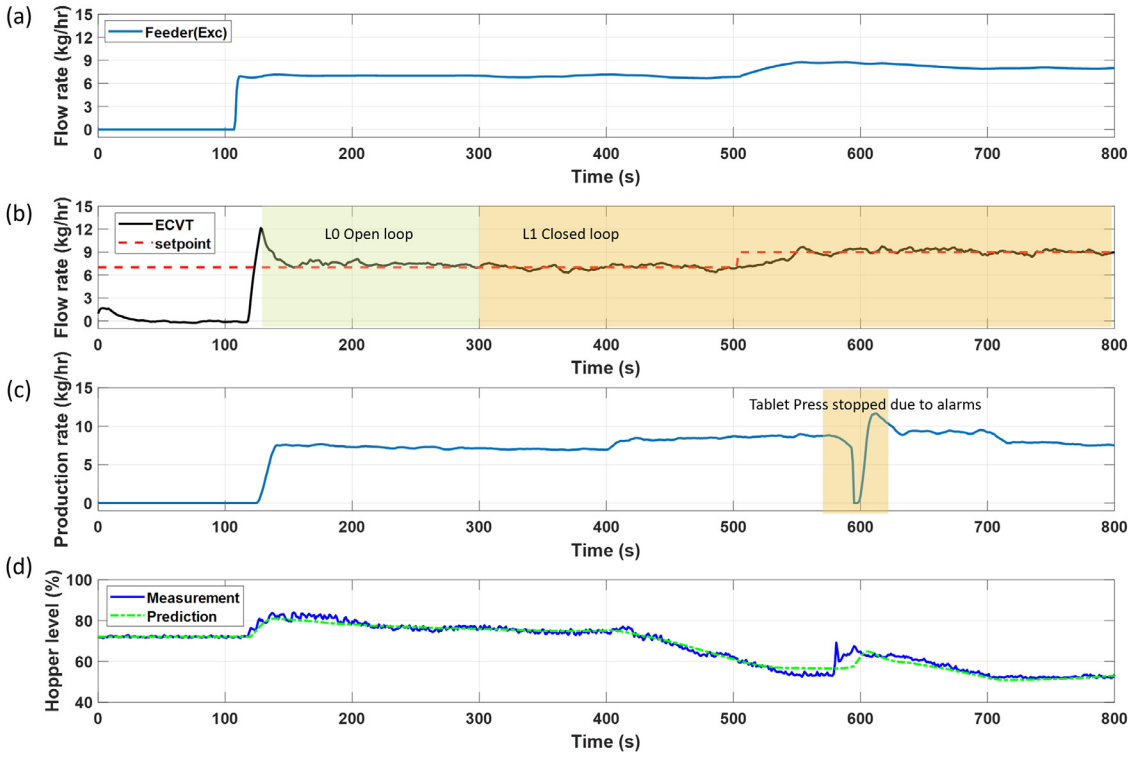

Fig. 8. Level 1 plant-wide control when only the excipient feeder was used: (a) the flow rate reading from the LIW feeder, (b) the blend flow rate, (c) the tablet production rate, and (d) the hopper level.

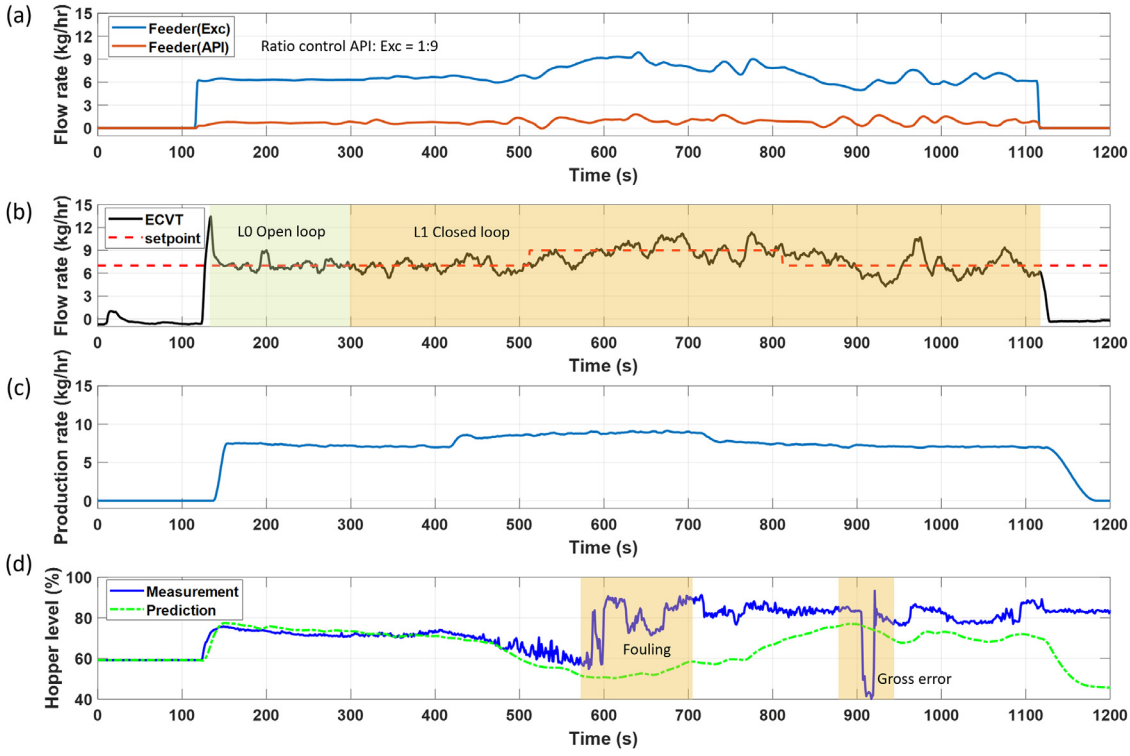

Fig. 9. Level 1 plant-wide control when both the excipient feeder and the API feeder were used: (a) the flow rate reading from LIW feeders, (b) the blend flow rate, (c) the tablet production rate, and (d) the hopper level.

predicted using the powder flow rate and the tablet production rate. When powder flow measurements and level measurements are not contaminated with powder fouling, the predicted hopper level can match level measurements well as shown in Fig. 8d.

Experimental Case Study 2: Both the Excipient and the API were Delivered

The API (APAP) flow was also incorporated into the process operation and a feedforward ratio controller was utilized to enable the ratio of the API flow to the excipient flow to be set at 1/9 as shown in Fig. 9a. The total powder flow can be controlled in the level 1 closed-loop operation as indicated in Fig. 9b, although the variation of the blend flow was larger compared to the total powder flow in case study 1. This was attributed to the fact that the poor flowability of APAP could cause ratholing and high flow variations, especially when the powder holdup in the feeder hopper was low and/or the set point was low. The poor flowability of APAP also deteriorated the accuracy of the measurement of the hopper level in the tablet press as shown in Fig. 9d. While the uniform LED backlight has been implemented to mitigate the effect of the dust and increase the contrast between the empty pipe and the accumulated powder, fouling caused by poor powder flowability still resulted in a bias in the level measurement. With the aid of inlet and outlet flow rate measurements, the predicted level can serve as an additional reference value when the level measurement is contaminated with the gross error.

In summary, integration of the mass flow sensor and even more PAT tools would not only increase the versatility of control design but also provide more process knowledge. With additional measurement redundancy, the collected process information will be more reliable using model-based approaches such as data reconciliation to deal with process uncertainty and plant-model mismatch, further increasing plant-wide control performance. The control performance depends on the sensor accuracy, and thus how to further improve the ECVT accuracy when powder fouling exists is worthy of investigation in the future. The use of a vibration device that does not interfere with sensor measurement is a possible solution to mitigate the effects of fouling. It may also be possible to implement additional electrode plates specifically designed to measure thin films of buildup on the pipe wall and use this information to correct the overall flow data. In addition, while direct level control in a feedback loop has not been applied in this work, level control indeed plays a key role to guarantee state of control over longer operation times. In the future, with reliable level estimation from using level measurements combined with flow measurements, the hopper level range can be maintained in a supervisory control loop by adjusting the setpoints for the inlet and outlet flow, further manipulating LIW feeder flow rates and the turret speed.

Conclusions

When real-time powder flow measurement is incorporated into the control structure, plant-wide control performance is significantly improved giving rise to smaller variations in CQAs compared to conventional strategies used in DC tablet production lines. Moreover, to achieve a fully automated process with uninterrupted operation, controlled holdup in each unit operation and a state of control are required especially in continuous manufacturing. Although direct level measurement of the tablet press hopper by image analysis might be compromised by powder fouling on the hopper wall, the hopper level can be predicted and thus the gross error of level measurements can be detected with the aid of real-time mass flow measurements. The aforementioned benefits depend on the accuracy of flow sensor measurements. To improve the accuracy of the ECVT sensor, sensor drift has been mitigated by the temperature correction method and powder fouling influence can be mitigated by the appropriate choice of pipe materials and addition of glidant. The ECVT sensor implemented in the DC line was able to capture the process dynamics in the intermediate flow downstream of the LIW feeders, showing great promise as a potential PAT for use in pharmaceutical continuous manufacturing processes.

Declaration of Competing Interest

The authors declare that they have no known competing financial interests or personal relationships that could have appeared to influence the work reported in this paper.

Acknowledgments

This work was supported by the United States Food and Drug Administration under grant 1U01FD006487-01.

Supplementary Materials

Supplementary material associated with this article can be found in the online version at doi:10.1016/j.xphs.2021.06.005.

References

1. Skibsted ETS, Westerhuis JA, Smilde AK, Witte DT. Examples of NIR based real time release in tablet manufacturing. *J Pharm Biomed Anal*. 2007;43(4):1297–1305.
2. Woodcock J. Modernizing pharmaceutical manufacturing–continuous manufacturing as a key enabler. In: *Proceedings of the International Symposium on Continuous Manufacturing of Pharmaceuticals*. Cambridge, MA; 2014.
3. Schaber SD, Gerogiorgis DI, Ramachandran R, Evans JMB, Barton PI, Trout BL. Economic analysis of integrated continuous and batch pharmaceutical manufacturing: a case study. *Ind Eng Chem Res*. 2011;50(17):10083–10092.
4. Ierapetritou M, Muzzio F, Reklaitis G. Perspectives on the continuous manufacturing of powder-based pharmaceutical processes. *AIChE J*. 2016;62(6):1846–1862.
5. Lee SL, O'Connor TF, Yang X, et al. Modernizing pharmaceutical manufacturing: from batch to continuous production. *J Pharm Innov*. 2015;10(3):191–199.
6. Yu LX, Amidon G, Khan MA, et al. Review article understanding pharmaceutical quality by design. *AAPS J*. 2014;16(4).
7. Matsunami K, Miyano T, Arai H, Nakagawa H, Hirao M, Sugiyama H. Decision support method for the choice between batch and continuous technologies in solid drug product manufacturing. *Ind Eng Chem Res*. 2018;57(30):9798–9809.
8. Su Q, Ganesh S, Moreno M, et al. A perspective on Quality-by-Control (QbC) in pharmaceutical continuous manufacturing. *Comput Chem Eng*. 2019;125:216–231.
9. Singh R, Sahay A, Karry KM, Muzzio F, Ierapetritou M, Ramachandran R. Implementation of an advanced hybrid MPC-PID control system using PAT tools into a direct compaction continuous pharmaceutical tablet manufacturing pilot plant. *Int J Pharm*. 2014;473(1–2):38–54.
10. Su Q, Bommireddy Y, Shah Y, et al. Data reconciliation in the Quality-by-Design (QbD) implementation of pharmaceutical continuous tablet manufacturing. *Int J Pharm*. 2019;563(April):259–272.
11. Kirchengast M, Celikovic S, Rehrl J, et al. Ensuring tablet quality via model-based control of a continuous direct compaction process. *Int J Pharm*. 2019;567:(858704) 118457.
12. Martinetz MC, Rehrl J, Aigner I, Sacher S, Khinast J. A continuous operation concept for a rotary tablet press using mass flow operating points. *Chemie-Ingenieur-Technik*. 2017;89(8):1006–1016.
13. Ganesh S, Troscinski R, Schmall N, Lim J, Nagy Z, Reklaitis G. Application of X-ray sensors for in-line and noninvasive monitoring of mass flow rate in continuous tablet manufacturing. *J Pharm Sci*. 2017;106(12):3591–3603.
14. Madarász L, Köte Á, Gyürkés M, et al. Videometric mass flow control: a new method for real-time measurement and feedback control of powder micro-feeding based on image analysis. *Int J Pharm*. 2020;580:(January) 119223.
15. Stranzinger S, Faulhammer E, Li J, et al. Predicting capsule fill weight from in-situ powder density measurements using terahertz reflection technology. *Int J Pharm X*. 2019;1:(October 2018) 100004.
16. Rao SM, Zhu K, Wang C-H, Sundaresan S. Electrical capacitance tomography measurements on the pneumatic conveying of solids. *Ind Eng Chem Res*. 2001;40 (20):4216–4226.
17. Li J, Bi D, Jiang Q, Wang H, Xu C. Online monitoring and characterization of dense phase pneumatically conveyed coal particles on a pilot gasifier by electrostatic-capacitance-integrated instrumentation system. *Measurement*. 2018;125:1–10.
18. Jaworski AJ, Dyakowski T. Application of electrical capacitance tomography for measurement of gas-solids flow characteristics in a pneumatic conveying system. *Meas Sci Technol*. 2001;12(8):1109.
19. Yan Y. Mass flow measurement of bulk solids in pneumatic pipelines. *Meas Sci Technol*. 1996;7(12):1687. Available at: http://stacks.iop.org/0957-0233/7/i=12/a=002. Accessed July 5, 2021..

20. Warsito W, Marashdeh Q, Fan L. Electrical capacitance volume tomography. *IEEE Sens J*. 2007;7(4):525–535.
21. Wang D, Xu M, Marashdeh Q, Straiton B, Tong A, Fan L. Electrical capacitance volume tomography for characterization of gas – solid slugging fluidization with Geldart Group D particles under high temperatures. *Ind Eng Chem Res*. 2018;57(7):2687–2697.
22. Weber JM, Bobek MM, Breault RW, Mei JS, Shadle LJ. Investigation of core-annular flow in an industrial scale circulating fluidized bed riser with electrical capacitance volume tomography (ECVT). *Powder Technol*. 2018;327:524–535.
23. Park HC, Choi HS. Visualization of flow structures inside a conical spouted bed by electrical capacitance volume tomography. *Particuology*. 2019;42:15–25.
24. Wang F, Marashdeh Q, Wang A, Fan LS. Electrical capacitance volume tomography imaging of three-dimensional flow structures and solids concentration distributions in a riser and a bend of a gas-solid circulating fluidized bed. *Ind Eng Chem Res*. 2012;51(33):10968–10976.
25. Agrawal V, Shinde YH, Shah MT, Utikar RP, Pareek VK, Joshi JB. Estimation of bubble properties in bubbling fluidized bed using ECVT measurements. *Ind Eng Chem Res*. 2018;57(24):8319–8333.
26. Weber JM, Mei JS. Bubbling fluidized bed characterization using electrical capacitance volume tomography (ECVT). *Powder Technol*. 2013;242:40–50.
27. Wang A, Marashdeh Q, Fan LS. ECVT imaging of 3D spiral bubble plume structures in gas-liquid bubble columns. *Can J Chem Eng*. 2014;92(12):2078–2087.
28. Sines JN, Straiton BJ, Zuccarelli CE, et al. Study of gas-water flow inside of a horizontal passive cyclonic gas-liquid phase separator system using displacement-current phase tomography. *Gravit Sp Res*. 2020;6(2):28–43.
29. Wang A, Marashdeh Q, Motil BJ, Fan LS. Electrical capacitance volume tomography for imaging of pulsating flows in a trickle bed. *Chem Eng Sci*. 2014;119:77–87.
30. Sines JN, Hwang S, Marashdeh QM, et al. Slurry bubble column measurements using advanced electrical capacitance volume tomography sensors. *Powder Technol*. 2019;355:474–480.
31. Chandrasekera TC, Wang A, Holland DJ, et al. A comparison of magnetic resonance imaging and electrical capacitance tomography: an air jet through a bed of particles. *Powder Technol*. 2012;227:86–95.
32. Holland DJ, Marashdeh Q, Müller CR, et al. Comparison of ECVT and MR measurements of voidage in a gas-fluidized bed. *Ind Eng Chem Res*. 2009;48(1):172–181.
33. Wang F, Yu Z, Marashdeh Q, Fan LS. Horizontal gas and gas/solid jet penetration in a gas-solid fluidized bed. *Chem Eng Sci*. 2010;65(11):3394–3408.
34. Weber JM, Layfield KJ, VanEssendelft DT, Mei JS. Fluid bed characterization using electrical capacitance volume tomography (ECVT), compared to CPFD software's barracuda. *Powder Technol*. 2013;250:138–146.
35. Wang A, Marashdeh Q, Teixeira FL, Fan LS. Applications of capacitance tomography in gas-solid fluidized bed systems. *Ind Tomogr Syst Appl*. 2015:529–549. Published online.
36. Li T, Scicolone JV, Sanchez E, Muzzio FJ. Identifying a loss-in-weight feeder design space based on performance and material properties. *J Pharm Innov*. 2019. Published online.
37. Újvári G, Kok JF, Varga G, Kovács J The physics of wind-blown loess: implications for grain size proxy interpretations in Quaternary paleoclimate studies. *Earth-Sci Rev*154:247–278.
38. Pu Y, Mazumder M, Cooney C. Effects of electrostatic charging on pharmaceutical powder blending homogeneity. *J Pharm Sci*. 2009;98(7):2412–2421.
39. Scholten B. *The Road to Integration: A Guide to Applying the ISA-95 Standard in Manufacturing*. ISA; 2007.
40. *ANSI A. ISA-95.00.01-2010: Enterprise-Control System Integration–Part 1: Models and Terminology*. 2010. Published online.
41. Ganesh S, Su Q, Vo LBD, et al. Design of condition-based maintenance framework for process operations management in pharmaceutical continuous manufacturing. *Int J Pharm*. 2020;587:(July) 119621.
42. Burcham CL, Florence AJ, Johnson MD. Continuous manufacturing in pharmaceutical process development and manufacturing. *Ann Rev Chem Biomol Eng*. 2018;9:253–281.
43. Singh R, Ierapetritou M, Ramachandran R. System-wide hybrid MPC-PID control of a continuous pharmaceutical tablet manufacturing process via direct compaction. *Eur J Pharm Biopharm*. 2013;85(3 PART B):1164–1182.
44. Ramachandran R, Arjunan J, Chaudhury A, Ierapetritou MG. Model-based control-loop performance of a continuous direct compaction process. *J Pharm Innov*. 2011;6(4):249–263.
45. Su Q, Moreno M, Giridhar A, Reklaitis GV, Nagy ZK. A systematic framework for process control design and risk analysis in continuous pharmaceutical solid-dosage manufacturing. *J Pharm Innov*. 2017;12(4):327–346.